EVALUATION OF AEROSOL MAPPING METHODS USING AVIRIS IMAGERY

Christoph Popp[1] , Daniel Schläpfer[1], Stephan Bojinski[2], Michael Schaepman[3], and Klaus I. Itten[1]
University of Zurich, Switzerland

1   INTRODUCTION

Natural and anthropogenic aerosols affect solar electromagnetic radiation on its propagation through the Earth's atmosphere. Their influence is twofold, directly by reflecting, scattering or absorbing processes and indirectly serving as cloud condensation nuclei (King et al, 1999). These processes influence the radiation budgets significantly from local to global scales thereby forming a major uncertainty in climate models.

Remote sensing has in recent years become an important tool to determine aerosol properties thus leading to a better understanding of the role of aerosols in the atmosphere. Due to the possibility of providing spatially homogeneous data, airborne or spaceborne sensor measurements constitute a main achievement to other approaches (e.g., sun photometry). Further, quantification of atmospheric aerosol characteristics is also needed as input parameter for the atmospheric correction of imagery data since aerosols modulate the optical signal reflected from a surface target into the sensor's field of view. For those reasons, different methods for the image-based retrieval and spatial mapping of aerosol parameters have been developed. Their principles are strongly connected to number, position and width of spectral bands, ground sampling distance, repetition rate, and view angle of the particular sensor type (King et al, 1999, gives an overview).

The objective of this paper is the application of standard aerosol mapping methods using year 2000 AVIRIS data measured over the greater Los Angeles (USA) area. Moreover, a new technique especially developed for aerosol retrieval by means of imaging spectroscopy data named *Aerosol Retrieval by Interrelated Abundances* (ARIA) (Bojinski, 2003) is introduced as an alternative. Above mentioned methods are all based on the occurrence of dark surface types in the investigated area. A rural region in the Santa Monica Mountains as well as a flat urban area in the vicinity of downtown Los Angeles have been chosen as test sites. Both scenes contain various surface types. Columnar aerosol optical depth (τ_a) at 550 nm for different aerosol regimes is calculated using a look-up table approach. The retrieved results are validated using the MODIS level2 aerosol product and in relation to the terrain surface reflectance and structure.

---

[1]   *Department of Geography, RSL, University of Zürich, Winterthurerstr. 190, CH-8057 Zürich, Switzerland, Phone: +41 1 635 52 50, Fax: +41 1 635 68 46, E-mail: chpopp@geo.unizh.ch*

[2]   *Global Climate Observing System (GCOS) Secretariat, c/o WMO, Geneva, Switzerland*

[3]   *Wageningen University, Centre for Geo-Information, Wageningen, The Netherlands*

2   METHODOLOGY

Aerosols attenuate the radiation due to their diverse particle size distribution and chemical composition in a wide wavelength range, mainly in the ultraviolet and visible part, except for large dust particles whose signatures are diminishing with longer wavelengths. Scattering at aerosol particles can be described by the Mie scattering approximation. The aerosol optical depth (τa) describes the scattering and absorption of aerosols integrated over an atmospheric column.

The principle behind remote sensing of aerosol properties might be described using radiometric transfer equations. The contribution of radiance reflected by atmospheric aerosols into the sensors field of view over dark surfaces basically can be expressed as:

$$\rho_a (\lambda) = \rho_{app} (\lambda) - \rho_{ground} (\lambda), \tag{1}$$

where ρ_{app} is the apparent reflectance measured by the sensor and ρ_{ground} denotes the reflectance at a surface target. Equation 1 illuminates the importance of an appropriate presumption of $\rho_{ground}(\lambda)$ in case of deriving aerosol parameters. Dark surface types are chosen as ideal targets for the inversion of aerosol optical depth mainly because of three reasons: firstly, the lower $\rho_{ground}(\lambda)$ the better $\rho_{app}(\lambda)$ can be separated into a contribution of ground reflectance and a contribution of aerosol scattering; secondly, $\rho_{ground}(\lambda)$ might be estimated more precisely than for brighter targets with regard to absolute error; and third, absorption and backscattering of ground reflected radiance on aerosols can be neglected. Aerosol optical depth then is derived by upward-calculation of $\rho_{ground}(\lambda)$ for aerosol parameter variations carried out numerically by pre-calculated look-up tables.

1.1   Dark Target

The dark target approach requires the occurrence of dense dark vegetation in the investigated area (Kaufman and Sendra, 1988). For instance, trees or bushes are commonly dark in the visible part of the electromagnetic spectrum. In atmospherically uncorrected imagery, dark vegetation pixels are identified by a threshold of a vegetation index. The surface reflectance of these pixels can subsequently be approximated by 0.02 +/- 0.01 reflectance in the red VIS channel of a particular sensor.

1.2   MODIS Band Ratio

MODIS's band ratio method (Kaufman et al., 1997) is based on an empirical relationship between SWIR reflectance at λ=2.1 µm and visible reflectance at λ=0.66 µm and λ=0.49 µm for a large variety of natural surfaces. Compared to the VIS wavelength range where most aerosol interaction with electromagnetic radiance occurs, a weak aerosol effect in the SWIR region can be assumed. Candidate Pixels are masked in the SWIR by thresholding and assumed ground reflectance in the VIS are calculated using the empirical ratios.

1.3   ARIA

Dissimilar to the above mentioned methods, the *Aerosol Retrieval by Interrelated Abundances* (ARIA, Bojinski, 2003) now makes explicitly use of the high number of spectral channels provided by AVIRIS and other imaging spectrometry instruments. ARIA is based on unmixing of the spectrally contiguous sensor signal in the SWIR range using a priori defined land surface reflectance endmembers. The derived abundances are interrelated between VIS and SWIR spectral ranges, if spectral auto-correlation is given. In this case, the abundances are derived from unmixing in the SWIR and then are used with the same endmembers to re-mix an assumption on surface reflectance in the VIS.

1.4   Further Methods and Trends

The combination of high spectral resolution with high signal to noise ratio bears the potential for a variety of other promising approaches. A method comparable to the ARIA method has been developed for SeaWIFS data by Von Hoyningen-Huene et al. (2003). It iteratively mixes the surface reflectance from reference spectra in the VNIR spectral range on the basis of vegetation abundance, derived at the same spectral range. Good results have been reported for this method on SeaWIFS, but its implementation on AVIRIS data has not yet been performed and tested. Another option is the use of the oxygen absorption at 760nm to retrieve the total optical thickness as it is done with MOS-B on IRS-1 (Pflug et al., 1999; Zimmermann 1991). The method requires spectral resolution below 5 nm and therefore is not suited to be used with AVIRIS data. A further method has been developed for GLI on ADEOS-1 (Höller et al., 2003). It detects the strong aerosol signature in the UV bands between 380 and 420 nm to estimate the aerosol contents and aerosol single scattering albedo. Also that approach is not well suited for AVIRIS data as noise levels are high in these critical wavelength regions.

3   DATA BASIS

The NASA Airborne Visible/Infrared Imaging Spectrometer (AVIRIS) onboard a U-2 aircraft flew over the Californian coast line from downtown Los Angeles westward to Point Mugu near Oxnard on 16 September 2000 at 11.00 local time and on a nominal altitude of 20 km above sea level. The complete flight strip measures 95 km in length and 12.3 km in width covering a wide range of different surface types. The area is sun-illuminated from the south-east and is cloud-free.

For comparison of aerosol retrieval methods, an urban and a mainly rural region have been chosen as test areas, in the following referred to as 'City' and 'Topanga' scene. Further, a USGS digital elevation model (DEM) with a spatial resolution of 10 m is used for orthorectification and atmospheric processing of the imagery.

Figure 1 illustrates the described AVIRIS image, the positioning of the two selected scenes as well as the corresponding digital elevation model in the lowest panel. The 'Topanga' scene includes mountainous areas of the Santa Monica Mountains to the north and west reaching terrain heights around 700 meters above sea level. These hilly areas are mostly covered by chaparral and dry bush lands, some small patches of bare soil also show up, most probably the result of periodic bush fires in this region. To the southeast, urban areas sprawl into the Santa Monica Mountains. To the south and west, the Pacific Ocean clearly is divided from the continent through a bright strip of sandy beaches.

The 'City' scene contains almost exclusively plane urban area with bigger patches of dark green vegetation which are mostly referred to as city parks. Here, brightness is proportional to building density. The Inglewood oil field at the southwestern boarder of the scene consists of bare soil with lowest average reflectance in the VIS.
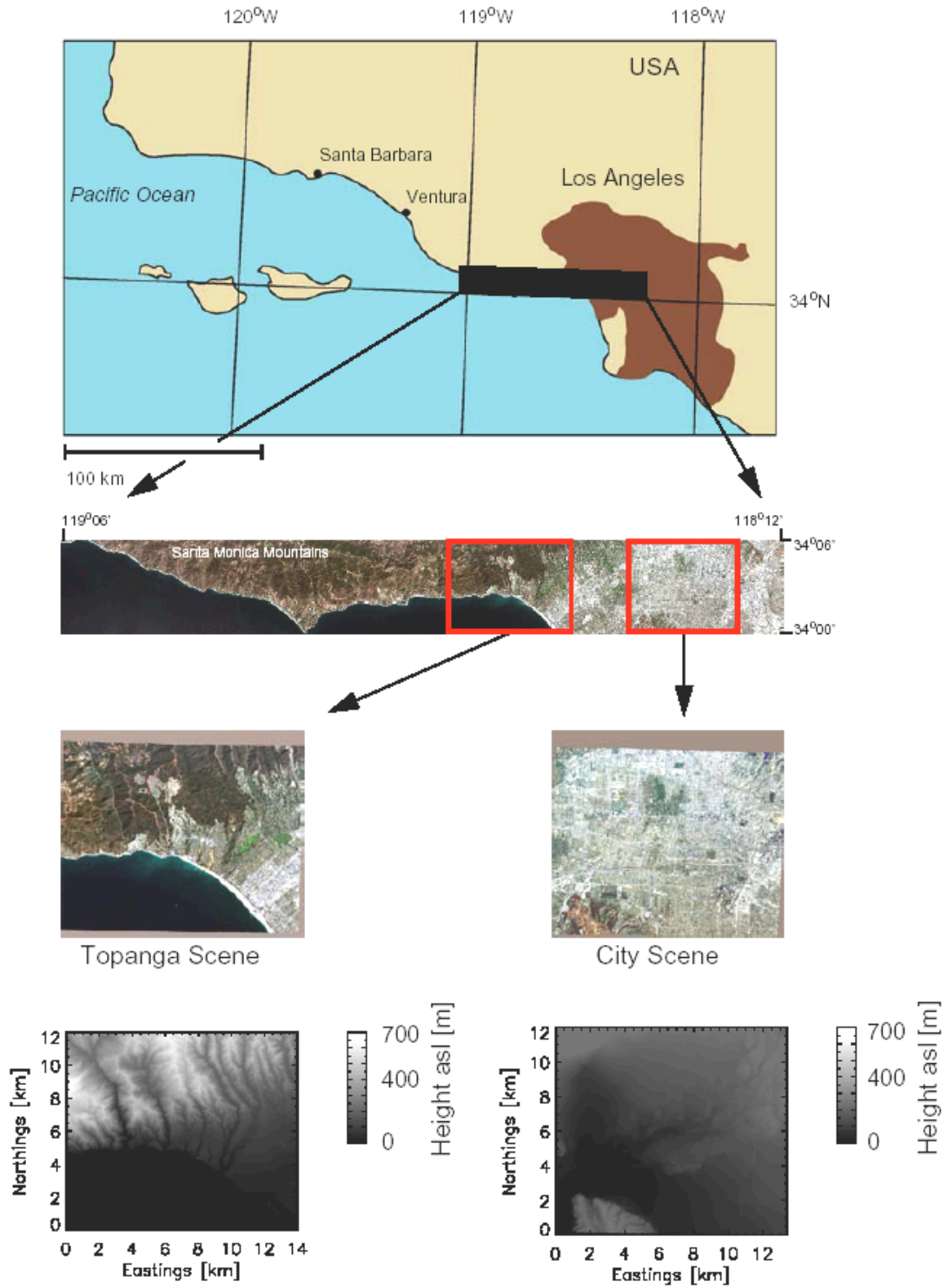
Figure 1: Location of the AVIRIS flight strip and the investigated scenes. In the lowest panel, the corresponding DEMs are shown.

4 APPLICATION USING AVIRIS IMAGERY

The imagery has been preprocessed in two steps. First an orthorectification is carried out with a parametric approach using the PARGE software (Schläpfer and Richter, 1998). Second, atmospheric processing of the imagery data is done using ATCOR-4 (Richter and Schläpfer, 2002). The atmospheric processing is done for two reasons: atmospheric correction with varying visibility and subsequent comparison to specific suitable and well-known endmember spectra (e.g. ocean water) can provide a first approximation of mean τ_a across a scene (τ_a and visibility are directly related). Aerosol optical depths in between 0.22 and 0.35 in combination with a maritime or rural aerosol type have been found by this method to be typical conditions. Secondly, the atmospheric preprocessing is done to remove Rayleigh scattering as height dependent disturbing factor. However, topographic correction has intentionally not been applied in order to keep the nature of shadowed areas as dark reference targets.

The calculation of look-up tables is performed using MODTRAN 4 (Berk et al., 1989) for a maritime, a rural as well as an urban aerosol model after Shettle and Fenn (1979) which are assumed to be the most dominant and plausible aerosol models in the investigated area. In this study, US standard atmosphere 1976 is used as input parameter in MODTRAN 4 and ATCOR-4.

To complement the later achieved aerosol mapping over land for all three methods, aerosol optical depth should also be derived over water surfaces for a spatially homogenous final aerosol map. A water mask is obtained setting thresholds of ρ_{app} (0.665) <= 0.02 and ρ_{app} (0.865) <= 0.02, respectively (Carrère et al., 1997). Water reflectance at λ=1.00 μm then is assumed to be 0.00 afterward being inverted using the pre-calculated look-up tables (Gao et al, 2000).

1.1 Dark Target

Identification of dense, dark vegetation pixels is achieved with the atmospherically resistant vegetation index (ARVI) (Kaufman and Tanré, 1992). The ARVI threshold is flexibly set such that 5% of the image pixels are classified. The darker half of these pixels in the NIR band finally is chosen as candidate pixels and their ρ_{ground} (0.665μm) is assumed to be 0.02 +/- 0.01.

1.2 Band Ratio

Masking of candidate pixels is done by setting two thresholds in the SWIR channel: a minimum of 0.005 reflectance avoiding the identification of water pixels for which this method does not work. A maximum of 0.05 reflectance is set such that at least 5% of the image pixels are selected. Otherwise this threshold is increased to 0.01. The overall brighter city scene requires the 0.01 threshold. To finish, an assumed ground reflectance in the red VIS is determined for every masked pixel applying the standard band ratio factor of 0.5 between SWIR and VIS band.

1.3 ARIA

Spectral autocorrelation has been investigated for spectral bands between 0.4 and 0.7 mm in the VIS, and the SWIR1 and SWIR2 region, respectively (Bojinski, 2003). Reflectance spectra for soil (895 spectra from a spectrum database), vegetation (1239), and rocks/minerals (917) surfaces have been analyzed. Averaged band correlations have been calculated. It has been revealed that for soil and vegetation, the SWIR1 and SWIR2 spectral ranges are uniformly correlated to the VIS part which has not been the case for rocks and minerals. Hence, rocks/mineral spectra are excluded from the analysis. Determining suitable candidate pixels for the inversion is done using the spectral angle mapper algo-

rithm (Richards and Jia, 1999). Spectral angles calculated between the atmospherically uncorrected image and one of the used endmember spectra equal or less than 0.15 are considered fitting. Next, the assumed VIS reflectance of the masked pixels is re-mixed using the abundances derived in the SWIR spectral region.

A spatially contiguous product finally is achieved by completing the land τ_a values with those derived over water followed by an interpolation of τ_a values to fill the gaps between pixels carrying aerosol information.

2   RESULTS, COMPARISON, AND DISCUSSION

2.1   Quantitative Validation

Aerosol optical depth is calculated for maritime, rural, and urban aerosol models for the dark target, band ratio, and ARIA method. Mean values of τ_a, their standard deviations, and the expectable errors for each result are illustrated in Table 1 for the Topanga scene and Table 2 for the City scene. For rural and maritime models, small differences can be observed in all categories. Use of the urban model yields values that stand noticeably apart in both scenes. In the dark target method, no average results could be determined as the fit of simulated to real data during the inversion process was inappropriate for the urban aerosol model. Maritime and rural results for mean τ_a in the dark target and the band ratio method are higher than for the ARIA method. In the Topanga scene, in-scene variations are approximately equally high for the dark target and ARIA methods, although at a higher overall τ_a level for the latter, and slightly higher for the band ratio method. In the city case, ARIA in-scene variation is lowest.

An urban aerosol regime does not seem to fit the atmospheric conditions the time the data has been collected. Considering maritime and rural results only, in absolute terms, the ARIA methods average error is smaller than in the dark target method and higher than in the band ratio method. Tolerable accuracies of $\Delta\tau a$ +/- 0.1 are exclusively attained by the band ratio retrieval in the Topanga scene for assumed rural and maritime aerosol regimes.

The given results seem to corroborate a similar performance of ARIA and band ratio method. It has to be noted, that all suited pixels have been included for the statistics. The ARIA method allows for aerosol detection on almost double the amount of pixels than the band ratio. If only the intersecting mask is evaluated, the performance of ARIA is clearly superior by a factor of 2 (i.e. standard deviations at 0.1-0.3 compared to 0.5-0.6 in $\Delta\tau a$).

Method	Aerosol	mean τ_a	stddev τ_a	$\Delta\tau_a$
ARIA	maritime	0.21	0.04	0.13
ARIA	rural	0.18	0.03	0.11
ARIA	urban	0.44	0.12	0.40
Band Ratio	maritime	0.24	0.06	0.10
Band Ratio	rural	0.23	0.06	0.10
Band Ratio	urban	0.56	0.22	0.32
Dark Target	maritime	0.30	0.04	0.18
Dark Target	rural	0.31	0.04	0.18
Dark Target	urban	-	-	-

Tab.1:Topanga scene results obtained with ARIA, band ratio, and dark target methods for different aerosol models.

Method	Aerosol	mean τa	stddev τa	$\Delta \tau a$
ARIA	maritime	0.28	0.09	0.15
ARIA	rural	0.25	0.08	0.14
ARIA	urban	0.86	0.51	1.49
Band Ratio	maritime	0.34	0.10	0.11
Band Ratio	rural	0.33	0.10	0.12
Band Ratio	urban	0.82	0.31	0.51
Dark Target	maritime	0.44	0.10	0.16
Dark Target	rural	0.47	0.10	0.17
Dark Target	urban	-	-	-

Tab.2: City scene results obtained with ARIA, band ratio, and dark target methods for different aerosol models.

2.2 Qualitative Validation

Figure 2 shows the interpolated and smoothed τa mapping results using a rural model for the three methods evaluated in this study for the Topanga scene and in the City scene, respectively. Dark water retrieval results are added to the raw aerosol map before interpolation. White areas denote unrealistic high τa values appearing where very few candidate pixels could be found. In the Topanga scene, the previously made conclusions are confirmed. The highest τa values can be found in urban or semi-urban areas in the eastern part of the image, the lowest are found in vegetated mountainous regions in the western part for all methods. All derived results show a relative strong correlation with geographically varying surface covers. This is not a very realistic representation of the spatial distribution of aerosols in the Earth's atmosphere since this rather depends on other factors (e.g., wind direction, aerosol size distribution). The highest overall τa values are retrieved using the dark target method, the lowest applying ARIA. Band ratio and ARIA maps show a similar structure, with stronger variability for the primary. Furthermore, red and blue areas are stronger speckled in the band ratio outcome. The dark target result seems smoother than the band ratio but includes significant higher τa values.

The aerosol inversion over water provides realistic uniform τa at reasonable absolute values. Artificially high τa values only show up along the coastline, most likely due to suspended matter or shallow water depths which undermine the dark water assumption. This might also explain the erroneously classified water pixels in the band ratio method. Assumed that aerosol concentrations usually do not change much on short distances, the contrast between over land and over ocean retrieved τa values can be considered as a supplementary criterion. Here, the dark target result shows the best fit whereas there are higher contrasts between ocean and vegetated areas in the other two methods.

In the City scene, applying the band ratio and the dark target methods, the highest τa values are found in areas including high building-density. The lowest τa values show up in the oil field with its low VIS reflectance in the southwest of the scene. The speckled and fragmentary resulting map from the band ratio and the dark target retrieval do not look very promising. The results appear most reasonable for the ARIA method, with relatively low spatial variation of τa. Compared to the Topanga scene, τa values in the City scene are significantly higher for the dark target and the band ratio method, except around some obviously low reflectance regions. This discrepancy cannot simply be assigned to higher air pollution in industrialized urban areas. It is rather a consequence of lacking appropriate dark pixels in the image. Because there are at least 5% of the image pixels chosen, these pixels are generally brighter than those chosen in the Topanga scene. For this reason, their real ground reflectance is strongly underestimated which finally leads to higher τa values.

A last criterion is the relation between aerosol mapping results and terrain shape. Lower aerosol load is expected at higher altitudes (compare Figure 1 for the digital terrain model). Here, only the Topanga scene can be evaluated. A certain relation between hill crests and aerosol contents can be

observed for both, the ARIA and the band ratio method. However, the interpolation routine applied to fill the gaps of non-evaluated pixels apparently reduces the terrain effect significantly. Much more obvious effects would be expected for a method working in a pixel-wise manner.
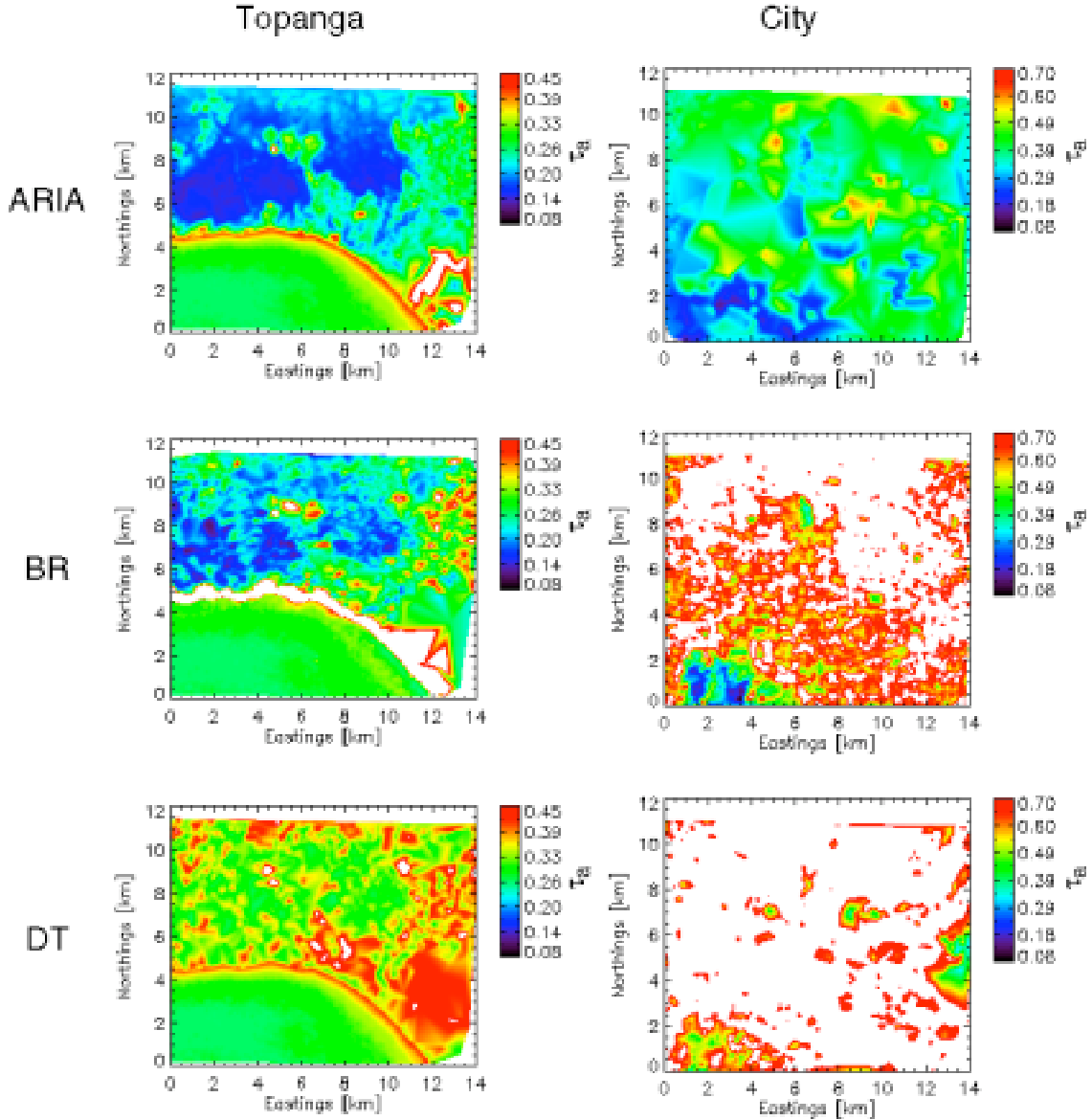
Figure 2: Final τa mapping results for ARIA, band ratio (BR) and dark target (DT) methods for an assumed rural aerosol model in the Topanga scene (left column) and the City scene (right column). White areas denote pixels with values that are considered unreasonably high. Aerosol optical depth values are given at 0.55 μm.

2.3   Validation with MODIS Data

Result qualities are assessed through indirect validation with the MODIS level 2 aerosol product due to lack of direct validation data such as sun photometry or other ground-based radiometric measure-

ments. The mean τ_a value obtained by the MODIS aerosol product for the Topanga scene is 0.08 +/- 0.07 and for the City scene 0.19 +/-0.09. The MODIS aerosol type is given as smoke for all pixels derived from geographically and seasonally defined climatology after d'Almeida et al. (1991). MODIS τ_a values are linearly interpolated for the centers of the Topanga and City scene on account of the large difference in scale – the ground resolution of the MODIS aerosol product is 25 km. Considerable differences can be observed between the results obtained in this study and the MODIS aerosol product. Generally, this may be due to the difference in scale. The ARIA results come closest to the reference product τ_a values. For the other two methods, not even the error bars overlap to those provided by the MODIS data. This cautiously verifies a slightly better quality of the ARIA method.

3   CONCLUSIONS

Aerosol optical depth has been derived for the same data using three different retrieval methods. Two traditional methods which make use of only a few spectral bands are compared to a recently developed method labeled ARIA which includes channels of a wider spectral range in order to determine atmospheric aerosol properties. An assumed urban aerosol model obviously does not represent atmospheric conditions during the data acquisition in none of the evaluated scenes. Results for maritime and rural aerosol regimes are at a comparable level for every inversion. Application of the traditional methods on areas with a lack of sufficient low reflectance surfaces in the VIS leads to unsatisfactorily results. In vegetated regions, their derived τ_a values are in expectable ranges taking visibility from the most conceivable a priori atmospheric correction as reference. The prospects of the dark target and the band ratio methods might rather be in fast image-based assessment of visibility values as input parameters for the atmospheric correction of remote sensing data, than in spatially homogenous aerosol mapping. Further, their applicability remains limited to areas with large parts of appropriate dark surface types.

In-scene smoothness is more reasonable for ARIA. In lack of suitable ground truth data, the MODIS level 2 aerosol product has been used for validation, whereas ARIA mean τ_a values showed best correspondences. Nevertheless, the calculated errors of every inversion are at high levels. Both of the methods provided adequate independency between surface cover reflectance and retrieved τ_a, which is relevant in interpolated gaps.

Particular methods and algorithms for remote sensing of aerosol parameters have to be developed in imaging spectroscopy with regard to more accurate and reliable spatial mapping of aerosols. The advancement of imaging spectrometer technology will lead to sensors allowing to make use of techniques whose potential is known but which cannot be applied to a sensor of AVIRIS type performance. The APEX system (e.g.; Schaepman et al., 2003) will offer full spectral coverage down to 380 nm at spectral resolutions below 5 nm, which allows for application of methods known from SeaWIFS, MOS-B, or GLI to full resolution imaging spectrometry data. A promising approach to be followed with APEX-type instruments is the evaluation of the oxygen feature in combination with the strong aerosol signatures at and below 400nm.

4   ACKNOWLEDGEMENTS

5 REFERENCES

Berk, A., Bernstein, L., and Robertson, D., 1989: *MODTRAN: a Moderate resolution Model for Lowtran7*. Technical Report, Spectral Sciences Inc., Burlington, Massachusetts, pp. 38.

Bojinski, S., 2003: *Imaging Spectroscopy of Aerosols using a Reference Spectrum Database*. PhD Thesis. Remote Sensing Series, Vol. 40. University of Zurich, Switzerland, pp.87.

Carrère, V., Dubuisson, P., Roger, J., and Santer, R., 1997: MERIS Level 2 Atmospheric Correction over Land : Pixel Identification, Data Simulation and Algorithm. Physical Measurements and Signatures in Remote Sensing V1. Ed. by G. Guyot & T. Phulpin, A.A. Balkema, Rotterdam, The Netherlands, pp. 27-37.

D'Almeida, G., Koepke, P., and Shettle, E., 1991: *Atmospheric Aerosols: Global Climatology and Radiative Characteristics*. Deepak, Hampton, Virginia, pp. 561

Gao, B., Montes, M., Ahmad, Z., and Davis, C., 2000: Atmospheric Correction Algorithm for Hyperspectral Remote Sensing of Ocean Color from Space. *Applied Optics*, 39(6):887-896.

Höller R., Higurashi A., Teruyuki N. and Nakajiama T.Y., 2003: Retrieval of aerosol optical thickness and single-scattering albedo over land from GLI, 35th conference of the remote sensing society of Japan. RSSJ, HIVE Nagaoka, Japan, pp. 275-276.

Kaufman, Y. and Sendra, C., 1988: Algorithm for Automatic Atmospheric Corrections to Visible and Near-IR Satellite Imagery. *International Journal of Remote Sensing*, 9(8):1357-1381.

Kaufman, Y. and Tanré, D., 1992: Atmospherically Resistant Vegetation Index (ARVI) for EOS-MODIS. *IEEE Transactions on Geoscience and Remote Sensing*, 30(2):261-270.

Kaufman, Y., Wald, A., Remer, L., Gao, B., Li, R., and Flynn, L., 1997: The MODIS 2.1-mm Channel-Correlation with Visible Reflectance for Use in Remote Sensing of Aerosol. *IEEE Transactions on Geoscience and Remote Sensing,* 35(5):1286-1297.

King, M., Kaufman, Y., Tanré, D., and Nakajima, T., 1999: Remote Sensing of Tropospheric Aerosols from Space: Past, Present, and Future. Bulletin of the American Meteorological Society, 80(11):2229-2259.

Pflug B., Krawczyk H. and Posse P., 1999: Atmospheric Ground Truth Measurements for Validation of MOS-Data and Angstrom Inversion Algorithm, 3rd International Workshop on MOS-IRS and Ocean Colour. Institute of Space Sensor Technology and Planetary Exploration, DLR, Berlin, pp. 121-129.

Richards, J. and Jia, X., 1999: *Remote Sensing Digital Image Analysis*. Springer-Verlag, Berlin, Germany, 3rd Edition, pp. 363.

Richter R. and Schläpfer D., 2002: Geo-atmospheric processing of airborne imaging spectrometry data. Part 2: Atmospheric/Topographic Correction. *International Journal of Remote Sensing*, 23(13): 2631-2649.

Schaepman M.E., Itten K.I., Schläpfer D., Kaiser J.W., Brazile J., Debruyn W., Neukom A., Feusi H., Adolph P., Moser R., Schilliger T., De Vos L., Brandt G., Kohler P., Meng M., Piesbergen J., Strobl P., Gavira J., Ulbrich G. and Meynart R., 2003: APEX: Current Status of the Airborne Dispersive Pushbroom Imaging Spectrometer. R. Meynart (Editor), International Symposium on Remote Sensing. *Sensors, Systems, and Next Generation Satellites VII*. SPIE, Barcelona, Vol. 5234, pp. 202-210.

Schläpfer D. and Richter R., 2002: Geo-atmospheric processing of airborne imaging spectrometry data. Part 1: Parametric Ortho-Rectification Process. *International Journal of Remote Sensing*, 23(13): 2609-2630.

Shettle, E. and Fenn, R., 1979: *Models for the Aerosols of the Lower Atmosphere and the Effect of Humidity Variations on their Optical Properties*. Technical Report AFGL-TR-79-0214, Air Force Geophysics Laboratory, Hanscom AFB, Massachusetts, pp. 94.

Von Hoyningen-Huene, W., M. Freitag, and J.P. Burrows, 2003: Retrieval of Aerosol Optical Thickness over Land Surfaces from Top-of-Atmosphere Radiance, *Journal of Geophysical Research-Atmospheres*, 108:4260.

Zimmermann G., 1991: *Fernerkundung des Ozeans*. Akademie Verlag, Berlin, pp. 419.